Combined In Vivo Confocal Raman Spectroscopy and Confocal Microscopy of Human Skin

P. J. Caspers,* G. W. Lucassen,† and G. J. Puppels*
*Erasmus MC, University Medical Center Rotterdam, Department of General Surgery, 3015 GE Rotterdam, The Netherlands; and †Personal Care Institute, Philips Research, 5656 AA Eindhoven, The Netherlands

ABSTRACT In vivo confocal Raman spectroscopy is a noninvasive optical method to obtain detailed information about the molecular composition of the skin with high spatial resolution. In vivo confocal scanning laser microscopy is an imaging modality that provides optical sections of the skin without physically dissecting the tissue. A combination of both techniques in a single instrument is described. This combination allows the skin morphology to be visualized and (subsurface) structures in the skin to be targeted for Raman measurements. Novel results are presented that show detailed in vivo concentration profiles of water and of natural moisturizing factor for the stratum corneum that are directly related to the skin architecture by in vivo cross-sectional images of the skin. Targeting of skin structures is demonstrated by recording in vivo Raman spectra of sweat ducts and sebaceous glands in situ. In vivo measurements on dermal capillaries yielded high-quality Raman spectra of blood in a completely noninvasive manner. From the results of this exploratory study we conclude that the technique presented has great potential for fundamental skin research, pharmacology (percutaneous transport), clinical dermatology, and cosmetic research, as well as for noninvasive analysis of blood analytes, including glucose.

INTRODUCTION

The human skin is layered. Conventionally the skin is described as divided in two major layers. The inner layer, the dermis, is between 1- and 4-mm thick. It consists mainly of connective tissue composed of collagen fibers. Other dermal structures include nerves, blood vessels, lymph vessels, muscles, and gland units. The outer layer, the epidermis, is typically ~40-μm thick, but it can be much thicker on load-bearing areas such as palms and soles. The epidermis can be divided in various sublayers. The principal cells of the epidermis are keratinocytes. These cells originate in the lower epidermis by division of basal cells in the basal layer. As the keratinocytes mature, they move upward toward the skin surface, thereby changing shape and molecular composition. Finally, the viable keratinocytes undergo a rapid, terminal transition into a cornified layer of dead, flattened cells, called the stratum corneum (SC) (Jakubovic and Ackerman, 1992; Odland, 1991). This outermost skin layer has a thickness of 10–15 μm on most areas of the body, except for the palms and the soles, where the SC can be more than 10 times thicker. Despite its normally minute thickness, the SC provides a highly efficient barrier for water and protection against microbial and chemical assault. The major constituent of the SC is keratin, which accounts for ~80% of its dry weight (Steinert and Freedberg, 1991).

Optical microscopic techniques offer unique possibilities for noninvasive skin research and skin characterization at high spatial resolution. Examples of such techniques are optical coherence tomography, two-photon fluorescence, and in vivo confocal scanning laser microscopy (CSLM). Optical coherence tomography takes advantage of the short temporal coherence of a broadband light source to reject multiple-scattered light. The spatial resolution in the axial direction is ~10–20 μm, which is close to the thickness of the stratum corneum (Huang et al., 1991; Schmitt et al., 1995) although more recently, depth resolutions better than 5 μm have been reported (Wang and Elder, 2002; Bordenave et al., 2002; Knuttel et al., 2001). Two-photon fluorescence microscopy uses two-photon excitation of endogenous chromophores in the tissue, which results in imaging with a high spatial resolution (Masters et al., 1998; Hendriks and Lucassen, 2001; So et al., 2000).

In vivo confocal microscopy enables real-time imaging of living tissue at high resolution and high contrast, without physically dissecting the tissue. The first in vivo confocal microscopic images of human skin were obtained with a tandem scanning confocal microscope. A mercury lamp was employed as light source and a Nipkow disk as scanning device (Corcuff and Leveque, 1993). Subsequently, CSLM has been developed, offering the advantage of precise wavelength selectivity and high illumination power (Rajadhyaksha et al., 1995). In vivo CSLM can be used to study the morphology of living skin for basic and clinical research. Confocal images show cellular and nuclear structure in the epidermis, collagen fibers in the dermis, and circulating blood cells in dermal capillaries, as well as structures such as sebaceous glands, hair and hair follicles, and sweat ducts. Different skin layers (stratum corneum, viable epidermis, dermis) can be clearly identified. In vivo confocal microscopy is a potential tool in the clinic for imaging skin lesions and their margins before biopsy, and for diagnosis of lesions (Rajadhyaksha et al., 1999).

These imaging techniques are methods to study skin morphology. In vivo confocal Raman spectroscopy provides detailed information about the molecular composition of the

Submitted October 11, 2002, and accepted for publication March 19, 2003.
Address reprint requests to Gerwin J. Puppels, E-mail: g.puppels@erasmusmc.nl.

0006-3495/03/07/572/09 $2.00

skin. Raman spectroscopy is widely used to study biological samples and, more recently, also to study the skin (Gniadecka et al., 1998; Barry et al., 1992). Application in clinical dermatology has been probed in studies of vitiligo (Schallreuter et al., 1999), atopic and psoriatic skin (Wohlrab et al., 2001), and basal cell carcinoma (Nijssen et al., 2002). We have introduced in vivo confocal Raman spectroscopy as a method to obtain depth-resolved information about the molecular composition of the skin (Caspers et al., 1998). The axial resolution of 5 μm (full width at half maximum) enabled the determination of in vivo concentration profiles of constituents of natural moisturizing factor (free amino acids and amino acid derivatives), of sweat (lactate and urea), and of water in the SC (Caspers et al., 2000, 2001, 2002).

In this paper we demonstrate that Raman spectroscopy for in vivo skin research can be further extended by combining the technique with CSLM. In this way, precise targeting of a (subsurface) skin structure for Raman measurements is enabled. In addition, molecular concentration profiles, as determined by Raman spectroscopy, can be directly related to skin architecture, in particular the skin layers.

MATERIALS AND METHODS

Instrumentation

Fig. 1 depicts the combined CSLM/Raman system. The system is based on a custom-built confocal Raman microspectrometer dedicated to in vivo examination of the skin (Caspers et al., 2000, 2001), and a confocal scanning laser microscope (type VivaScope 1000, Lucid Inc., Rochester, NY). The confocal Raman system employs a tunable titanium-sapphire laser (model 3900S, Spectra-Physics, Mountain View, CA) pumped by an Argon-ion laser (model 2020, Spectra-Physics). The spectra were recorded using a custom-designed F/2.1 spectrograph with 6 cm^{-1} spectral resolution and a liquid nitrogen cooled, deep depletion charge-coupled device (CCD) camera with a chip size of 1024 $\times$ 256 pixels (Princeton Instruments, Trenton, NJ). A 30$\times$ numerical aperture (NA) 0.90 water immersion microscope objective with coverglass correction was used (Lomo, Vermont Optechs, Charlotte, VT) to focus the laser light from both the Raman laser and the CSLM laser. The objective was mounted in a fast and accurate piezoelectric focusing drive, accurate to less than 0.1 μm operating in closed-loop (position-controlled) mode (Physik Instrumente, Waldbronn, Germany). Focusing of the microscope objective and adjustment of the power of the laser diode of the CSLM were controlled by a personal computer. This PC was also used to digitize and store the confocal images produced by the VivaScope. The operating software was custom developed (Philips Research, Eindhoven, The Netherlands). A second PC was used to record the Raman spectra.

The laser beam of the CSLM was focused to a diffraction limited spot, which was continuously scanned in two dimensions across the focal plane. The maximum field of view was 500 $\times$ 500 μm, using a 30$\times$ objective. The laser beam for Raman excitation was focused to a static diffraction limited spot in the center of the focal plane. The CSLM and the Raman system were optically coupled using a custom-designed filter inserted in the light path just above the microscope objective (see Fig. 1 *A*). An antireflection coated window is placed above the filter to correct for the parallel beam displacement caused by refraction at the filter surfaces (see Fig. 1 *B*). The coupling filter was designed to transmit the imaging laser beam of the CSLM (830 nm) and to reflect the Raman signal at wavelengths >850 nm. As described below, Raman measurements were performed using either 720 nm or 850 nm laser excitation. At both wavelengths, the filter transmitted a fraction of the laser light that was scattered by the skin (see Fig. 1 *C*). In this way the location of the focus of the Raman laser appears in the CSLM image. When the surface of a coverglass was imaged, the focus of the Raman laser appeared as a small, bright spot. The position of this spot was marked with a digital cross-hair in the video image. This was done because the focus of the Raman laser, while imaging the skin, was generally less bright and often difficult to distinguish from contrasting structures of the skin. With the cross-hair in place, the location of the focal point of the Raman laser was unambiguously marked, accurately indicating the location from which a Raman spectrum is obtained.

The standard operating procedure of the CSLM was applied, in which a coverglass was mounted in a metal ring that was stuck to the skin with double-sided tape. The metal ring was then attached to the microscope and could be moved laterally with a *xy*-translation stage. In this way a target of interest in the skin could be positioned in the focused laser beam for Raman spectroscopic evaluation. Because the skin was in contact with the coverglass, the distance between the microscope objective and the skin surface could be accurately controlled. Unintentional vertical motion of the skin could be limited to ~2 μm (Caspers et al., 2001). Coverglasses were made of CaF_2, because of its weak Raman signal in the spectral region of interest. Demineralized water between the coverglass and the skin surface was used to improve refractive index matching. This is of particular importance for the quality of the confocal images of the skin. Without water, a thin layer of air exists between coverglass and skin, resulting in large changes in the refractive index at the coverglass-air-skin interface. This would strongly degrade the image quality (Rajadhyaksha et al., 1999). The refresh rate of the CSLM images was 14 frames/s.

It was experimentally verified that the origin of the Raman signal was located within 2 μm of the focal plane of the CSLM. For this purpose polystyrene beads of 1-μm diameter were stuck to the coverglass of the CSLM and the surface of the coverglass was brought into the focal plane of the CSLM. A bead was positioned in the focused Raman laser by moving the coverglass laterally. Once the bead was in focus, the intensity of its Raman signal was monitored while the bead was moved through the focal plane in the axial direction. In this way it was determined that the maximum Raman signal was obtained when the bead was within 2 μm of the focal plane of the CSLM. This is well within the current axial resolution of the confocal Raman spectrometer in the combined system (9 μm). The axial resolution, defined as the full width at half maximum (FWHM) of the response curve of an infinitesimal thin plane, was determined from the derivative of a measured step response curve across an oil-CaF_2 interface. Details of this method have been described elsewhere (Caspers et al., 2000). In the current setup we used the standard microscope objective that was provided with the VivaScope (30$\times$ NA 0.9 water immersion). The combination of magnification and NA of the microscope objective, the focal length of the lens in front of the signal collection fiber, and the core diameter of this fiber (see Fig. 1 *A*) was not fully optimized. Therefore, the axial resolution for the Raman measurements was worse than the 5-μm resolution achieved in previous studies (Caspers et al., 2000).

In all in vivo experiments the depth, or distance to the skin surface, was determined from the displacement of the piezoelectric drive relative to the zero position, at which the focal plane was at the skin surface. No attempt was made to correct for a focus shift in the axial direction due to refractive index differences between water, the coverglass, and skin (Rajadhyaksha et al., 1999).

Experiments

In vivo experiments were carried out on the volar aspect of the arm and on the palm of the hand of healthy volunteers. The skin was not pretreated in any way. Approval for these experiments was obtained from the Medical Ethics Review Board of the Erasmus MC.

In vivo concentration profiles of water and constituents of sweat and natural moisturizing factor (NMF) were determined as follows. Raman spectra were recorded from a range of depths across the SC of the palm, from the skin surface down to the viable epidermis. Depth increments were

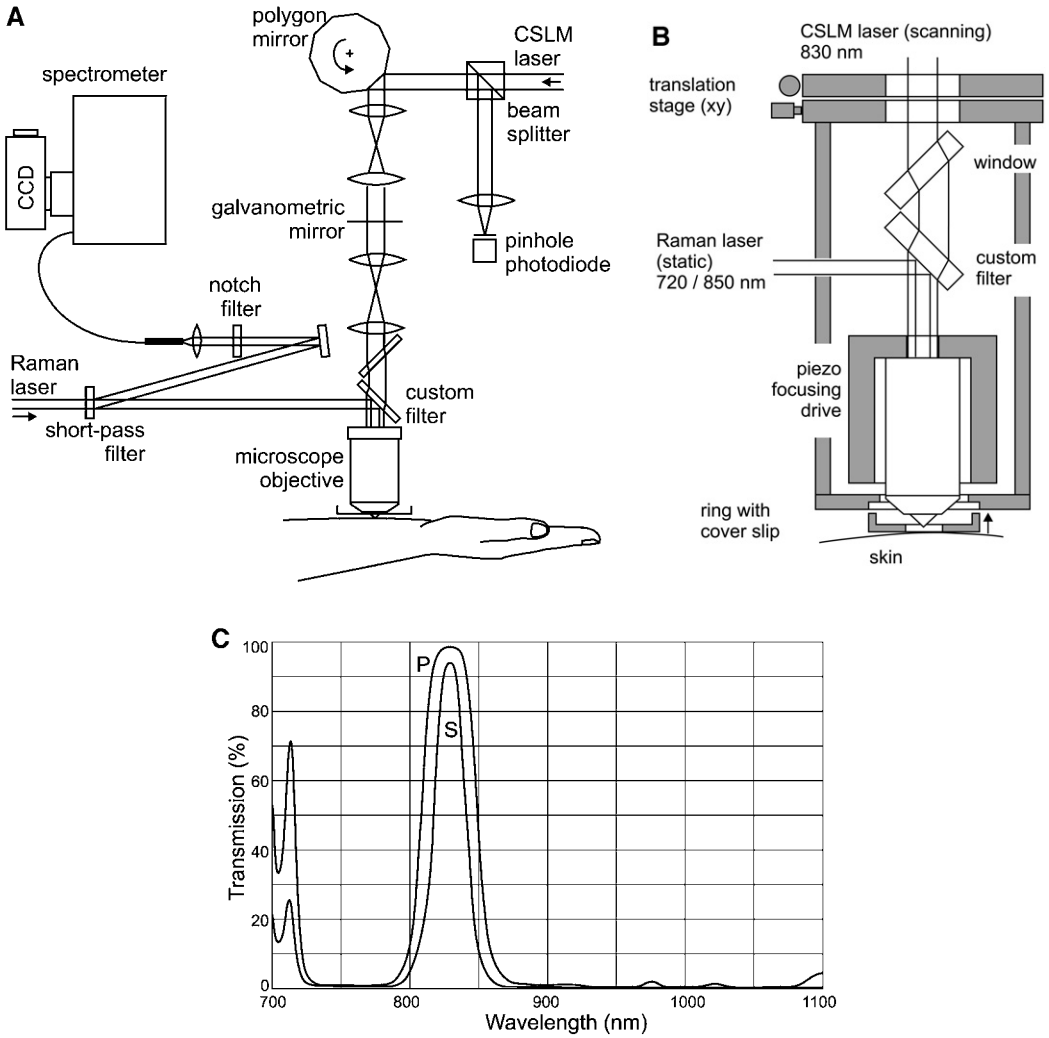

FIGURE 1 Combined confocal scanning laser microscope and confocal Raman spectrometer for in vivo study of the skin. (*A*) Schematic overview of the setup. Light from the Raman laser (720 nm and 850 nm) was transmitted by a short-pass filter and reflected by a custom-designed filter (transmission curve shown in Fig. 1 *C*), which partially reflected light at wavelengths 720 nm and 850 nm and completely reflected Raman scattered light with wavelengths >850 nm. The light was then focused to a diffraction limited spot by a microscope objective. Scattered light was collected by the same objective and reflected by the custom filter and by the short-pass filter. The scattered light was filtered by a laser rejection filter and focused onto the 100-μm core of an optical fiber, using an f = 149 mm achromat. The core of the optical fiber served as a confocal pinhole, rejecting out-of-focus light. The output of the fiber was connected to a spectrograph. Laser light from the CSLM, produced by an 830-nm diode laser, was transmitted by the custom filter and focused by the microscope objective to a diffraction limited spot, which was scanned across the focal plane. (*B*) Detailed view of the coupling between the CSLM and the Raman system. (*C*) Transmission curve of the coupling filter between the CSLM and the Raman spectrometer for parallel (P) and normal (S) polarization. Angle of incidence: 45°.

typically 10 μm. A corresponding set of CLSM images was used to visualize the boundary between the SC and the viable epidermis. Images were recorded at depth intervals of 1 μm. The images were stored on disk and processed afterwards to obtain an in vivo cross-sectional image of the SC and part of the viable epidermis.

For determination of water concentrations in the SC, a laser wavelength of 720 nm was used for Raman excitation. Raman spectra were recorded at 1 s per spectrum in the wavenumber region from 2000 to 4000 cm^{-1}. From these Raman spectra, water concentration profiles were determined. The water concentration in mass percentage was calculated using the intensity ratio between the Raman bands of water (3350–3550 cm^{-1}) and protein (2910–2965 cm^{-1}). The details of this procedure are described elsewhere (Caspers et al., 2000, 2001).

For the determination of concentration profiles of NMF and sweat constituents, Raman spectra were recorded in the spectral region from 400–2000 cm^{-1} (''fingerprint region''). The excitation wavelength in these experiments was 850 nm. The data collection time was 30 s per spectrum. Concentration profiles of NMF were determined semiquantitatively, using the relative signal contributions of NMF and keratin to the total in vivo Raman spectrum of stratum corneum (~80% of the dry weight of the stratum corneum consists of keratin). This was done using multiple-least-squares fitting, in which the in vivo skin spectrum was fitted with the in vitro Raman spectra of NMF, keratin, ceramide, lactate, and urea. A combination of these in vitro Raman spectra provides an adequate model for in vivo spectra of human SC (Caspers et al., 2001). The resulting fit coefficients represent the relative proportions in which these species contribute to the

total SC Raman signal. The NMF/keratin ratio was the ratio between the fit coefficients of NMF and keratin. This ratio was normalized to 1 at the maximum value.

Raman spectra of structures in the skin (sweat ducts, sebaceous glands, and blood capillaries) were measured in the fingerprint region. The excitation wavelength was 850 nm and the exposure time was 20 s per spectrum. Together with each recorded Raman spectrum, the corresponding CSLM image was captured and stored. For comparison with in vivo Raman spectra of dermal capillaries, in vitro spectra were recorded from fresh, human blood in glass capillaries. In all in vivo experiments the Raman laser power at the skin was 100 mW.

Data processing

The software used to control the CSLM enabled automatic recording and storage of confocal images as a stack of uncompressed bitmap files. For easy handling, a descriptor file was generated containing the filenames and depth coordinates for each image in a stack. A complete stack represents a volume section of the tissue, with each pixel having an (x,y,z)-coordinate and a brightness level. Plotting the image stack in an xy-plane (that is, all pixels having the same z-coordinate) results in an image of a section parallel to the skin surface. Similarly, cross-sectional images were obtained by plotting the image stack in an xz-plane or in a yz-plane.

Processing of images and of spectral data was done with software that was developed in-house using Matlab (MathWorks, Natick, MA). The Raman spectra were calibrated to relative wavenumbers and corrected for the wavelength dependent detection efficiency of the Raman system (Wolthuis et al., 1999).

RESULTS

Fig. 2 *A* shows an in vivo cross-sectional image (xz-plane) of the skin at the palm of the hand obtained with the CSLM, and a water concentration profile obtained simultaneously by Raman spectroscopy. The water concentration profile was determined from the Raman spectra that were measured on the dashed line. The solid line demarcates the boundary between the SC and the stratum granulosum (SG), at a depth of 145 μm below the skin surface. The confocal image in the xy-plane obtained at this position is shown in Fig. 2 *B*. Clearly visible are the uppermost cells of the stratum granulosum at the SC/SG junction. Fig. 2 shows a result that is representative of the results obtained in 10 experiments in which water concentration profiles were measured using Raman spectroscopy in combination with CSLM.

A similar experiment was carried out to determine the (semiquantitative) concentration profile of NMF in relation to skin architecture. Fig. 3 *A* shows an in vivo cross-sectional image (xz-plane) of the skin at the palm of the hand obtained with the CSLM, and a concentration profile of natural moisturizing factor profile obtained simultaneously by Raman spectroscopy. The NMF concentration was determined as a ratio (in arbitrary units) between the intensities of the Raman signal contributions of NMF and keratin, where keratin is the main constituent of the SC. The dashed line indicates the line on which the Raman spectra were recorded. The solid line indicates the SC/SG boundary. Fig. 3 *B* shows a confocal image in the xy-plane that was obtained at this position. The result here is representative for the results of a total of eight experiments in which the NMF profiles were measured in combination with CSLM.

Fig. 4 shows a confocal image of a sweat duct in the SC of the thenar at 30 μm below the skin surface. Several Raman spectra were recorded in and around the sweat duct. Spectra from the center of the sweat duct, and from the area around the sweat duct are plotted next to the image. Clear spectral differences can be observed, of which the intensity difference seen in the Raman band at 856 cm^{-1} (marked with an *asterisk*; see Discussion) is the most prominent.

Fig. 5 shows a confocal section of a sebaceous gland located on the lower forearm at a depth of 15 μm below the skin surface. Several Raman spectra were recorded in and around the gland. A typical spectrum from the gland and a typical spectrum from the area around the gland are shown next to the image. A prominent spectral difference, the Raman band at 1296 cm^{-1}, is marked with an asterisk (see Discussion).

In the lower part of the epidermis, dermal papillae can be observed. These structures show up in a CSLM image as bright circles around a darker central part (Rajadhyaksha et al., 1995). Blood flow within dermal capillaries can be observed in the center of dermal papillae. These capillaries

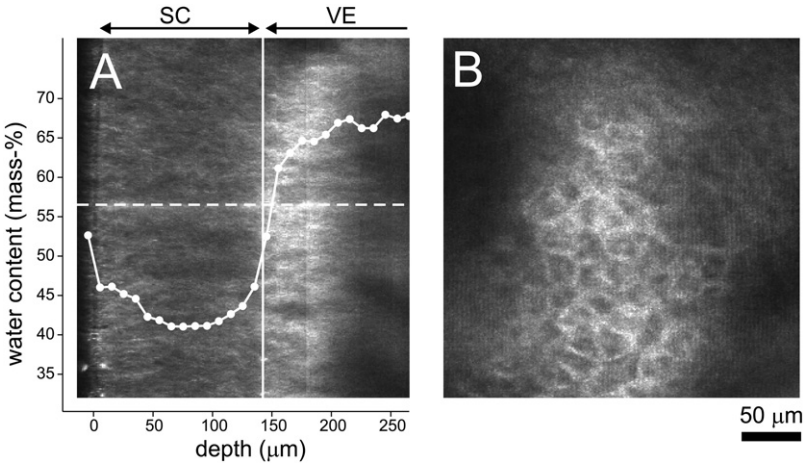

FIGURE 2 In vivo confocal images and a water concentration profile for the stratum corneum of the palm, based on combined CSLM and Raman measurements. (*A*) Cross section of the skin (xz-plane; SC: stratum corneum; VE: viable epidermis). Plotted in the image is the water concentration profile as determined from Raman measurements on the dashed line. The x axis represents the distance to the skin surface and applies to both the image and the graph. The y axis represents the water concentration in mass percentage (grams of water per 100 g of wet tissue). The solid line locates the plane from which image *B* was obtained. (*B*) Confocal image parallel to the skin surface (xy-plane), recorded at 145 μm below the skin surface at the boundary between SC and VE.

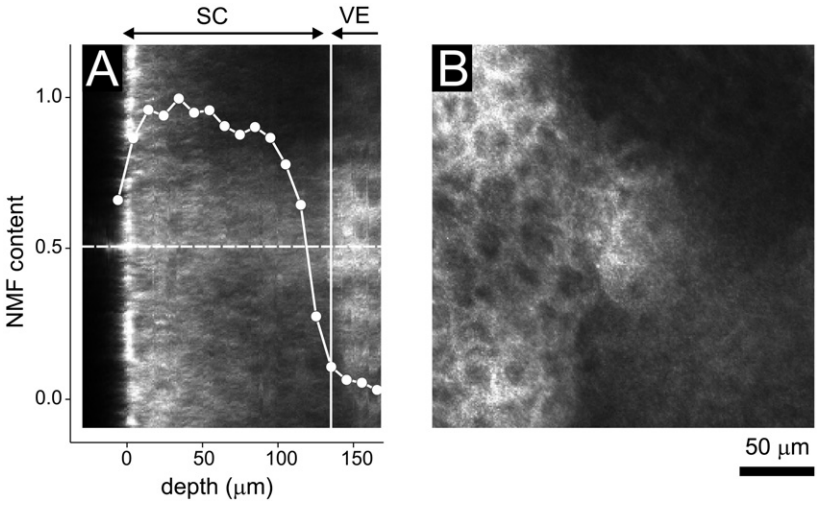

FIGURE 3 In vivo confocal images and a concentration profile of NMF for the stratum corneum of the palm. (*A*) Cross section of the skin (*xz*-plane; SC: stratum corneum; VE: viable epidermis). Plotted in the image is the relative amount of NMF as a function of depth, as determined from Raman measurements on the dashed line. The *x* axis represents the distance to the skin surface and applies to both the image and the graph. The *y* axis represents the relative amount of NMF, normalized to its maximum value. The solid line locates the plane from which image *B* was obtained. (*B*) Confocal image parallel to the skin surface (*xy*-plane) recorded 135 μm below the skin surface at the boundary between SC and VE.

ascend from the papillary plexus, which is a network of microcirculatory elements oriented parallel to the skin surface. The plexus is located in the upper part of the dermis. From this plexus, capillary loops are directed toward the epidermis and extend into the dermal papillae (Jakubovic and Ackerman, 1992). Fig. 6 shows a confocal image of a dermal capillary. Although capillaries may be difficult to recognize in a single image, they clearly show up in the live video image because of the circulating blood cells, which appear as bright dots moving along the same path (Rajadhyaksha et al., 1995). By positioning capillaries in the center of the cross-hair, Raman spectra were obtained of blood inside the capillary. Fig. 6 shows an in vivo spectrum obtained from a capillary and for comparison, a spectrum of blood that was obtained in vitro.

DISCUSSION

In the in vivo cross-sectional CSLM images of the palm (Figs. 2 *A* and 3 *A*), the skin surface and the junction between the SC and the viable epidermis can be easily observed. Contrast in CSLM originates from differences in the amount of back-scattered light from structures in the skin. The amount of back-scattered light largely depends on variations in refractive index within the tissue (Rajadhyaksha et al., 1995). However, the SC is an optically homogeneous layer; the cells are flattened, and nuclei and other cell organelles are absent. As a result CSLM images of the SC are relatively dark and show little contrast. In comparison, the living cells of the viable epidermis contain cytoplasm, organelles, and nuclei, from which light is scattered due to refractive index changes. Overall, images of the viable epidermis are therefore brighter than images of the SC. As a result, the cross-sectional image shows a well-defined junction between the darker SC and the brighter viable epidermis (Figs. 2 *A* and 3 *A*).

The water concentration profile in the SC provides insight into the water-holding capacity and barrier properties of the skin. This has implications for pharmacology, cosmetics, and fundamental skin biology. Transepidermal water loss measurements and skin impedance measurements have been used in combination with mathematical modeling of water diffusion through a membrane to study the barrier properties

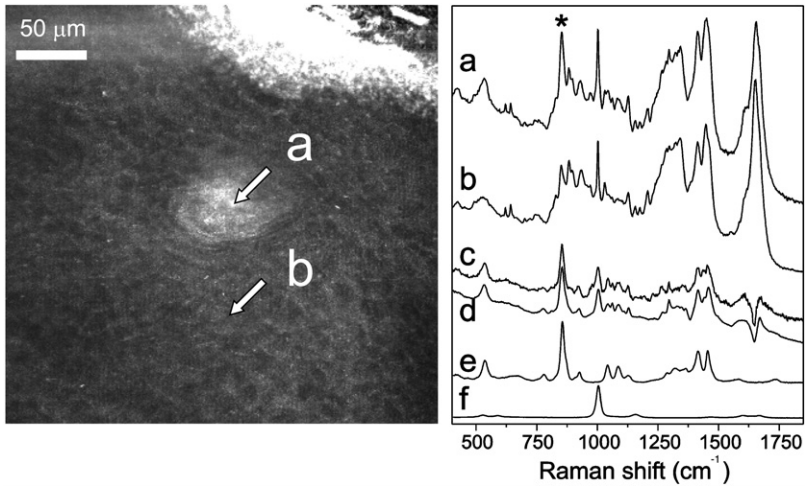

FIGURE 4 In vivo confocal image and Raman spectroscopy of a sweat duct on the palm of the hand, 30 μm below the skin surface. The bright area is a sweat duct. The arrows (*left*) mark the spots from which the Raman spectra were obtained. The asterisk marks the prominent Raman band of lactate at 856 cm^{-1} (see text). (*a, right*) Raman spectrum measured in the sweat duct. (*b, right*) Raman spectrum measured outside the sweat duct. (*c, right*) Difference spectrum (a minus b). (*d, right*) Fit result of spectrum a with spectrum b and spectra of NMF and sweat constituents (see text for details). (*e, right*) In vitro Raman spectrum of lactate. (*f, right*) In vitro Raman spectrum of urea.

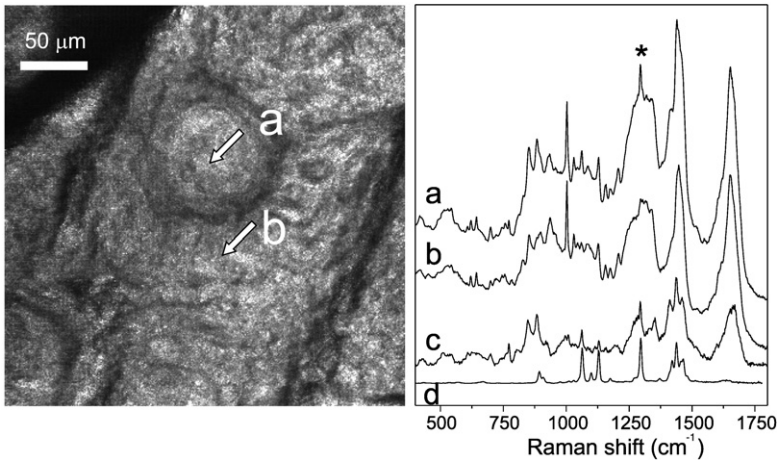

FIGURE 5 In vivo confocal image and Raman spectroscopy of a sebaceous gland on the lower forearm, 15 μm below the skin surface. The arrows (*left*) mark the spots from which the Raman spectra were obtained. The asterisk marks the prominent Raman band of lipid at 1296 cm^{-1}. (*a, right*) Raman spectrum measured in the sebaceous gland. (*b, right*) Raman spectrum measured outside the gland. (*c, right*) Difference spectrum (a minus b). (*d, right*) In vitro Raman spectrum of palmitic acid.

of the SC (Kalia et al., 1996; Schwindt et al., 1998). These studies have provided indirect information about the location of the water barrier and the water concentration profile. However, they have not resulted in a clear understanding of the in vivo water concentration in the SC as a function of depth.

In contrast, confocal Raman spectroscopy combined with CSLM provides a direct method to study the water concentration profile in the SC. With the results presented here, we show for the first time a detailed in vivo water concentration profile for the SC in relation to the skin architecture. The water concentration within the SC of the palm is constant throughout most of the SC (Fig. 2). Only at the junction between the SC and viable epidermis does the water content increase with a steep gradient, reaching ~70% (mass %, or grams of water per 100 g of wet tissue) in the viable epidermis. The slight increase of the water content at the skin surface has not been observed in earlier experiments using in vivo confocal Raman spectroscopy without CSLM (Caspers et al., 2000, 2001) and must be dismissed as an artifact. It is presumably caused by the thin film of water between the window and the skin surface that was applied to improve optical refractive index matching between skin surface and coverglass (see Materials and Methods section). The use of a different matching medium, such as oil, would avoid this problem. The presence of a steep gradient at the lower part of the SC implies that the water barrier is not homogeneously distributed over the entire SC of the palm, but located mostly at the junction between the SC and the SG. These observations do not confirm results obtained by transepidermal water loss measurements and mathematical modeling from which it was concluded that the SC of the arm is a homogeneous water barrier (Kalia et al., 1996; Schwindt et al., 1998). Whether the in vivo water concentration profile for the SC of the arm has the same pattern of a slowly varying water concentration in most of the SC followed by a steep gradient at the lower SC boundary remains to be elucidated. Currently the axial resolution of the combined Raman/CSLM system is not sufficient to answer this question, but an improvement with a factor of 3 to ~3 μm is feasible.

The relative changes in the concentration of NMF show a pattern quite different from the water concentration profile. Scott and co-workers have shown that a layer of stable filaggrin exists in the lowermost cell layers of the SC (Scott and Harding, 1986; Rawlings et al., 1994). This precursor protein is broken down by hydrolytic enzymes, a process that produces the free amino acids and amino acid derivatives that, together with specific salts, form the NMF. Proteolytic

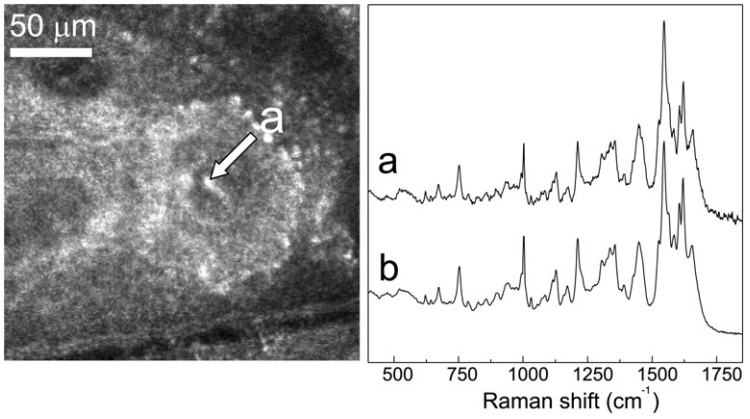

FIGURE 6 In vivo confocal image and Raman spectrum of a dermal capillary in the skin of the lower forearm. The depth is 60 μm below the skin surface. The arrow (*a*, *left*) indicates the location from which the Raman spectrum was obtained. (*a, right*) In vivo Raman spectrum of blood measured directly in a dermal capillary. Signal integration time: 30 s. (*b, right*) In vitro spectrum of blood.

activity of these enzymes is modulated by the water content in the tissue. Radio labeling and immunohistochemical studies in rats have shown that a high-water content in the SC prevents the production of NMF by filaggrin proteolysis. In normal conditions, the relatively dry external environment dries out the outer layers of the SC resulting in a water gradient decreasing from the deeper SC toward the surface. The decreased water content triggers proteolysis of filaggrin in the deeper part of the SC (Scott and Harding, 1986).

Fig. 3 visualizes this localized production of NMF in the lower part of the SC in vivo. The NMF-to-keratin ratio is zero in the viable epidermis. The steep gradient in the NMF profile indicates a very rapid increase of NMF at $\sim$15 μm above the SC/SG junction. According to Fig. 2, the water concentration at the distance of $\sim$15 μm from the SC/SG junction has dropped considerably with respect to the water concentration in the viable cells. These in vivo observations are in agreement with the findings by Scott and co-workers (Scott and Harding, 1986) that a decrease in water concentration is required before the proteolysis of filaggrin can start and the presence of NMF can be detected.

Absence or decreased production of NMF has been related to skin problems such as xerosis, ichtyosis, and psoriasis (Horii et al., 1989; Rawlings et al., 1994). Decrease in NMF has also been observed in aged skin (Rawlings et al., 1994). In vivo confocal Raman spectroscopy combined with CSLM provides a method to study the distribution of NMF and water in the SC in vivo. It can therefore contribute to gaining insight into the cause and treatment of skin conditions such as those mentioned above.

Figs. 4–6 illustrate the capability of combined confocal Raman spectroscopy and CSLM for study of the molecular composition of structures in the skin in situ. The real-time imaging capability of the CSLM was used to locate a structure of interest, such as a sweat duct (Fig. 4). Confocal Raman spectroscopy was then used to obtain spectroscopic information from this structure. Clearly the Raman band at 856 cm^{-1} is more intense in the spectrum of the sweat duct (*a, right*) than in the spectrum measured outside the duct (*b, right*). Multiple regression fitting of spectrum a with spectrum b and the spectra of lactate, urea, and the predominant constituents of NMF was applied to interpret these spectral differences in terms of differences in molecular composition. Details of the fitting procedure have been described elsewhere (Caspers et al., 2001). The choice of these constituents for fitting purposes is based on the assumption that NMF, which is highly water soluble and present in high concentrations in the SC, can easily dissolve in sweat (Sato et al., 1991). Lactate and urea are also present in sweat, as both are secreted by the sweat glands. The concentrations usually depend on the sweat rate. At low sweat rates, the concentration of lactate can be as high as 40 mM and that of urea 4 mM (Sato et al., 1991). At the current spatial resolution of the instrument, signal from the tissue surrounding the sweat duct also unavoidably is collected. Therefore, spectrum b (Fig. 4) was also included in the fit to the spectrum obtained in the sweat duct. The difference spectrum and the fit with the aforementioned compounds (Fig. 4) showed that the concentration of lactate in the sweat duct is much higher than in the surrounding tissue. The significance of this result is that it demonstrates that information about the molecular composition of sweat can be obtained from a sweat duct in situ. For cosmetic research, in designing and improving antiperspirants, which involves modulation of sweat production, this may offer a new and valuable tool to study the effects of these formulations in situ.

A similar experiment was carried out for a sebaceous gland, located at the lower forearm. Human sebaceous glands secrete a lipid mixture of mainly triglycerides, wax esters, free fatty acids, and squalene (Stewart and Downing, 1991). The process of sebogenesis is complex and not entirely understood. It involves elongation and desaturation of free fatty acids in the sebaceous cells, and incorporation of free fatty acids into triglycerides and wax esters. At a later stage bacterial hydrolysis of triglycerides causes the release of free fatty acids.

The Raman spectrum (Fig. 5) from the sebaceous gland (*a, right*) shows a strong band at 1295 cm^{-1}, which is not present in the spectrum recorded outside the gland (*b, right*). The difference spectrum (*c, right*) shows many Raman bands, indicating a difference in molecular composition between the sebaceous gland and the skin around the gland. Although the Raman bands of spectrum a (*a, right*) remain to be assigned, the comparison with the spectrum of palmitic acid (*d, right*) suggests the presence of this 16-carbon fatty acid in the sebaceous gland. The 16-carbon acids are predominant in sebaceous cells (Pappas et al., 2002). This first result demonstrates the potential to study the lipid composition in a sebaceous gland in vivo. It also suggests the possibility to measure Raman spectra in various parts of the sebaceous gland, which would enable one to follow the complex process of sebogenesis in vivo.

Confocal Raman spectroscopy combined with an imaging modality such as CSLM can be used to obtain direct chemical information about structures in the skin in situ. As such, the technique presented also provides a potential method to investigate in vivo the penetration of topically applied substances via shunt routes. This offers the possibility to apply substances to the skin and study their effects in situ, directly in the sebaceous glands, sweat glands, or hair follicles. This capability should be of particular interest in cosmetics research and pharmaceutical research on transdermal drug delivery.

In vivo recording of Raman spectra from dermal capillaries (Fig. 6) offers possibilities that reach well beyond skin research. Spectrum a was recorded in vivo, focusing on a capillary, whereas spectrum b is an in vitro spectrum of blood. The in vivo spectrum a is likely to contain signal contributions from the surrounding tissue, but clearly the

majority of the spectrum originates from blood flowing through the dermal capillary. The collection time for spectrum a was only 30 s, demonstrating that high-quality Raman spectra of blood can be rapidly measured in a completely noninvasive manner.

The Raman spectrum of blood largely depends on the oxygenation state of hemoglobin (Venkatesh et al., 1999; Wood and McNaughton, 2002). Due to the high spatial resolution of both CSLM and in vivo confocal Raman spectroscopy, it seems feasible to study the local hemoglobin-oxygen saturation at a microscopic scale. This is currently being investigated. Several in vitro studies have shown the feasibility of using Raman spectroscopy to determine analyte concentrations in whole blood, in plasma, or in serum (Pilotto et al., 2001; Berger et al., 1997; Berger et al., 1999). We therefore believe that the new technique presented here, enabling the in vivo recording of Raman spectra from dermal capillaries, has great potential for noninvasive monitoring of blood analytes, including glucose.

CONCLUSIONS

The combination of confocal Raman microspectroscopy and CSLM has been presented as a novel noninvasive method to obtain information about molecular composition in relation to skin architecture. CSLM is an imaging modality that can be used to image specific structures in the skin and to generate in vivo cross-sectional images of the skin. By combining CSLM with confocal Raman microspectroscopy, we show that detailed information about molecular composition can be obtained from well-defined regions in the confocal image. This was demonstrated by obtaining in vivo concentration profiles of water and of NMF in the SC that were directly related to the layered skin architecture by simultaneous recording of cross-sectional images of the skin. The possibility of studying the molecular composition of specific skin structures in vivo (sweat duct, sebaceous gland, dermal capillary) also was demonstrated. We believe that the technique presented provides the basis for a wide range of applications in fundamental skin research, as well as in pharmacology, dermatology, and cosmetics. The fact that high-quality spectra of blood can be obtained rapidly and completely noninvasively supports our great expectations for in vivo confocal Raman microspectroscopy in combination with CSLM as a method for noninvasive blood analysis.

REFERENCES

Barry, B. W., H. G. M. Edwards, and A. C. Williams. 1992. Fourier Transform Raman and infrared vibrational study of human skin: assignment of spectral bands. *J. Raman Spectrosc.* 23:641–645.

Berger, A. J., I. Itzkan, and M. S. Feld. 1997. Feasibility of measuring blood glucose concentration by near-infrared Raman spectroscopy. *Spectrochim. Acta A.* 53:287–292.

Berger, A. J., T. W. Koo, I. Itzkan, G. Horowitz, and M. S. Feld. 1999. Multicomponent blood analysis by near-infrared Raman spectroscopy. *Appl. Opt.* 38:2916–2926.

Bordenave, E., E. Abraham, G. Jonusauskas, N. Tsurumachi, J. Oberle, C. Rulliere, P. E. Minot, M. Lassegues, and J. E. S. Bazeille. 2002. Wide-field optical coherence tomography: imaging of biological tissues. *Appl. Opt.* 41:2059–2064.

Caspers, P. J., G. W. Lucassen, H. A. Bruining, and G. J. Puppels. 2000. Automated depth-scanning confocal Raman microspectrometer for rapid in vivo determination of water concentration profiles in human skin. *J. Raman Spectrosc.* 31:813–818.

Caspers, P. J., G. W. Lucassen, E. A. Carter, H. A. Bruining, and G. J. Puppels. 2001. In vivo confocal Raman microspectroscopy of the skin: noninvasive determination of molecular concentration profiles. *J. Invest. Dermatol.* 116:434–442.

Caspers, P. J., G. W. Lucassen, R. Wolthuis, H. A. Bruining, and G. J. Puppels. 1998. *In vitro* and *in vivo* Raman spectroscopy of human skin. *Biospectroscopy.* 4:S31–S39.

Caspers, P. J., A. C. Williams, E. A. Carter, H. G. M. Edwards, B. W. Barry, H. A. Bruining, and G. J. Puppels. 2002. Monitoring the penetration enhancer dimethylsulfoxide in human stratum corneum by in vivo confocal Raman spectroscopy. *Pharm. Res.* 19:1577–1580.

Corcuff, P., and J. L. Leveque. 1993. In vivo vision of the human skin with the tandem scanning microscope. *Dermatology.* 186:50–54.

Gniadecka, M., O. Faurskov Nielsen, D. H. Christensen, and H. C. Wulf. 1998. Structure of water, proteins, and lipids in intact human skin, hair, and nail. *J. Invest. Dermatol.* 110:393–398.

Hendriks, R. F. M., and G. W. Lucassen. 2001. Two-photon fluorescence and confocal video microscopy of in-vivo human skin. *In* Multiphoton Microscopy in Biomedical Sciences. A. Periasamy and P. T. So, editors. SPIE, San Jose, CA. 287–293.

Horii, I., Y. Nakayama, M. Obata, and H. Tagami. 1989. Stratum corneum hydration and amino acid content in xerotic skin. *Br. J. Dermatol.* 121:587–592.

Huang, D., E. A. Swanson, C. P. Lin, J. S. Schuman, W. G. Stinson, W. Chang, M. R. Hee, T. Flotte, K. Gregory, C. A. Puliafito and J. G. Fujimoto. 1991. Optical coherence tomography. *Science.* 254:1178–1181.

Jakubovic, H. R., and A. B. Ackerman. 1992. Structure and function of skin: development, morphology, and physiology. *In* Dermatology. S. L. Moschella and H. J. Hurley, editors. W. B. Saunders Company, Philadelphia. 3–87.

Kalia, Y. N., F. Pirot, and R. H. Guy. 1996. Homogeneous transport in a heterogeneous membrane: water diffusion across human stratum corneum in vivo. *Biophys. J.* 71:2692–2700.

Knuttel, A., S. Bonev, A. Hoepfner, and C. Kugler. 2001. Sub-surface skin imaging and evaluation by Optical Coherence Tomography (OCT). *J. Invest. Dermatol.* 117:962.

Masters, B. R., P. T. So, and E. Gratton. 1998. Multiphoton excitation microscopy of in vivo human skin. Functional and morphological optical biopsy based on three-dimensional imaging, lifetime measurements and fluorescence spectroscopy. *Ann. N. Y. Acad. Sci.* 838:58–67.

Nijssen, A., T. C. Bakker Schut, F. Heule, P. J. Caspers, D. P. Hayes, M. Neumann, and G. J. Puppels. 2002. Discriminating basal cell carcinoma from its surrounding tissue by Raman spectroscopy. *J. Invest. Dermatol.* 119:64–69.

Odland, G. F. 1991. Structure of the skin. *In* Physiology, Biochemistry and Molecular Biology of the Skin. L. A. Goldsmith, editor. Oxford University Press, New York. 3–62.

Pappas, A., M. Anthonavage, and J. S. Gordon. 2002. Metabolic fate and selective utilization of major fatty acids in human sebaceous gland. *J. Invest. Dermatol.* 118:164–171.

Pilotto, S., M. T. Pacheco, L. Silveira, Jr., A. B. Villaverde, and R. A. Zangaro. 2001. Analysis of near-infrared Raman spectroscopy as a new technique for a transcutaneous non-invasive diagnosis of blood components. *Lasers Med. Sci.* 16:2–9.

Rajadhyaksha, M., S. Gonzalez, J. M. Zavislan, R. R. Anderson, and R. H. Webb. 1999. In vivo confocal scanning laser microscopy of human skin II. Advances in instrumentation and comparison with histology. *J. Invest. Dermatol.* 113:293–303.

Rajadhyaksha, M., M. Grossman, D. Esterowitz, R. H. Webb, and R. R. Anderson. 1995. In vivo confocal scanning laser microscopy of human skin: melanin provides strong contrast. *J. Invest. Dermatol.* 104:946–952.

Rawlings, A. V., I. R. Scott, C. R. Harding, and P. A. Bowser. 1994. Stratum corneum moisturization at the molecular level. *J. Invest. Dermatol.* 103:731–741.

Sato, K., W. H. Kang, and F. Sato. 1991. Eccrine sweat glands. *In* Physiology, Biochemistry and Molecular Biology of the Skin. L. A. Goldsmith, editor. Oxford University Press, New York. 741–762.

Schallreuter, K. U., J. Moore, J. M. Wood, W. D. Beazley, D. C. Gaze, D. J. Tobin, H. S. Marshall, A. Panske, E. Panzig, and N. A. Hibberts. 1999. In vivo and in vitro evidence for hydrogen peroxide (H2O2) accumulation in the epidermis of patients with vitiligo and its successful removal by a UVB-activated pseudocatalase. *J. Investig. Dermatol. Symp. Proc.* 4:91–96.

Schmitt, J. M., M. J. Yadlowsky, and R. F. Bonner. 1995. Subsurface imaging of living skin with optical coherence microscopy. *Dermatology.* 191:93–98.

Schwindt, D. A., K. P. Wilhelm, and H. I. Maibach. 1998. Water diffusion characteristics of human stratum corneum at different anatomical sites in vivo. *J. Invest. Dermatol.* 111:385–389.

Scott, I. R., and C. R. Harding. 1986. Filaggrin breakdown to water binding compounds during development of the rat stratum corneum is controlled by the water activity of the environment. *Dev. Biol.* 115:84–92.

So, P. T. C., C. Y. Dong, B. R. Masters, and K. M. Berland. 2000. Two-photon excitation fluorescence microscopy. *Annu. Rev. Biomed. Eng.* 2:399–429.

Steinert, P. M., and I. M. Freedberg. 1991. Molecular and cellular biology of keratins. *In* Physiology, Biochemistry and Molecular Biology of the Skin. L. A. Goldsmith, editor. Oxford University Press, New York. 113–147.

Stewart, M. E., and D. T. Downing. 1991. Chemistry and function of mammalian sebaceous lipids. *Adv. Lipid Res.* 24:263–301.

Venkatesh, B., S. Ramasamy, M. Mylrajan, R. Asokan, P. T. Manoharan, and J. M. Rifkind. 1999. Fourier transform Raman approach to structural correlation in hemoglobin derivatives. *Spectrochim. Acta A.* 55A:1691–1697.

Wang, R. K., and J. B. Elder. 2002. High resolution optical tomographic imaging of soft biological tissues. *Laser Phys.* 12:611–616.

Wohlrab, J., A. Vollmann, S. Wartewig, W. C. Marsch, and R. Neubert. 2001. Noninvasive characterization of human stratum corneum of undiseased skin of patients with atopic dermatitis and psoriasis as studied by Fourier transform Raman spectroscopy. *Biopolymers.* 62:141–146.

Wolthuis, R., T. Bakker Schut, P. Caspers, H. Buschman, T. Roemer, H. Bruining, and G. Puppels. 1999. Raman spectroscopic methods for in vitro and in vivo tissue characterization. *In* Fluorescent and Luminescent Probes for Biological Activity. W. Mason, editor. Academic Press, London. 433–455.

Wood, B. R., and D. McNaughton. 2002. Micro-Raman characterization of high- and low-spin heme moieties within single living erythrocytes. *Biopolymers.* 67:259–262.